FEASIBILITY STUDY OF INDUCING DESIRABLE RESIDUAL STRESS DISTRIBUTION IN LASER MICROMACHINING

Wenwu Zhang and Y. Lawrence Yao
Department of Mechanical Engineering
Columbia University, New York, NY 10027

ABSTRACT

Laser machining/micromachining normally induces in the target material a residual stress distribution, which may favor microcrack propagation leading to reduced fatigue life of the material. This paper investigates the feasibility of introducing the effect of laser shock processing (LSP), that is, imparting a compressive residual stress distribution into the target material, into laser micromachining processes. Following a brief review of the principles and modeling aspects of LSP, various possibilities of such introduction were discussed and its feasibility was experimentally and numerically shown.

1. INTRODUCTION

In laser materials processing such as laser machining/micromachining, target material inevitably undergoes intensive non-uniform temperature changes and as a result a complex residual stress distribution forms near the processed area. An unfavorable stress distribution may result in microcrack formation and propagation, reduce the part's fatigue life, and lead to catastrophic failures. For this reason, studies were carried out to investigate such process effects.

Thermally induced stress in laser drilling and scribing of ceramics was studied (Modest, 1997; Modest and Thomas, 1999). Their simulations show that there exists a very thin region of compressive residual stress at the surface of the hole, while substantial tensile stresses develop over a thick layer below and parallel to the surface. Numerical analysis of the heat affected zone and residual stress distributions for laser cutting of stainless steel was investigated (Li and Sheng, 1995; Sheng and Joshi, 1995). Their simulation results based on an in-plane model show that along the cutting edge there is a high level of tensile stress that sharply reverts to compressive stress once away from the edge. The sharp stress gradient was thought to make the cutting edge susceptible to micro/macro crack formation.

If such processes can be altered in some fashion, one will have control over the resultant residual stress distribution at least to some extent. Laser shock processing (LSP) may potentially offer the possibility of doing so. LSP has been studied on and off since 1970s (Clauer, et al., 1981; Peyre, et al., 1996), in which laser generated shock waves in a confining medium are used to improve the mechanical properties of metallic materials including aluminum, steel and copper alloys. In particular, LSP induces compressive residual stress in the target and improves its fatigue life. Lasers of 1.06 μm wavelength and 1-6 mm beam size are commonly used in conventional LSP.

In this paper, basic principles and some modeling aspects of LSP are briefly explained followed by discussions on possible introduction of the LSP effects into laser micromaching processes. Experimental and numerical considerations are then given. In the section on results and discussion, experimental validation of the LSP simulation model is first reported, the resultant residual stress distribution is discussed, and the simulation is extended to pre-drilled, pre-grooved target geometry. Finally, laser micromachining experiments aimed at having the LSP effects are carried out to demonstrate the feasibility of such introduction.

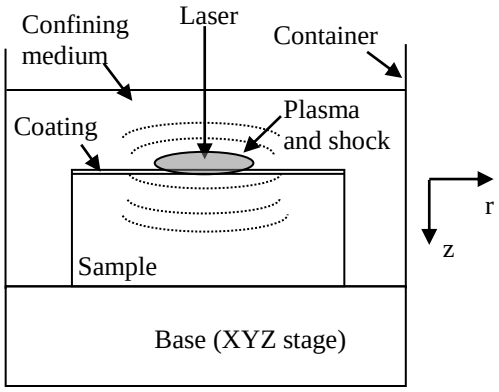

Figure 1 Illustration of laser shock processing

2. BASIC PRINCIPLES OF LASER SHOCK PROCESSING

In order to investigate possible introduction of the effect of LSP in laser machining/micromaching processes, the basic principles of LSP are briefly explained below. As illustrated by Fig. 1, when a short and intense (>1 GW/cm^2) laser pulse is irradiated onto a metallic target, the surface layer instantaneously vaporizes into a high temperature and high pressure (~1-10 GPa) plasma. This plasma induces shock waves during expansion from the irradiated surface, and mechanical impulses are transferred to the target. If the plasma is not confined, i.e., in open air, the pressure can only reach several tenths of one GPa. If it is confined by a liquid (e.g., water) or another type of medium, the shock pressure can be magnified by a factor of 5 or more compared with the open-air condition (Fox, 1974). At the same time, the shock pressure lasts 2 to 3 times longer than the laser pulse duration. Most LSPs also use a coating to protect the target from thermal effects so that nearly pure me-

chanical effects are induced. The coating could be metallic foil, organic paints or adhesives. These coatings can modify the surface loading transmitted to the substrate by acoustic impedance mismatch effects at the coating-substrate interface, and an additional 50% increase in the peak stress values can be achieved (Peyre, et al., 1998). Pressures above 1 GPa are above the yield stress of most metals, thus plastic deformation can be induced. If the peak shock pressure is over the *HEL* (Hugoniot Elastic Limit) of the target material for a suitable time duration, compressive stress distribution in the irradiated volume can be formed (Clauer, et al., 1981). The beam spot size used was in the order of millimeters and the compressive stress typically reached about one millimeter into the target material.

3. MODELING ASPECTS OF LASER SHOCK PROCESSING

In LSP, the target is subjected to strong shock pressures (typically >1 GPa), the interaction time is short (<100 ns), and the strain rate is high (>10^5 s^{-1}). As a result, some aspects of modeling are briefly discussed below. The changes necessary for the micro scale of interest in this paper, are also explained.

3.1 Shock pressure

Earlier modeling work on laser-induced shock waves was carried out by Clauer, et al. (1981). Their model considered the non-linear coupled irradiation and hydrodynamic equations governing pressure evolution at the metal surface. Fabbro, et al. (1990) developed a model, which assumes that the laser irradiation is uniform and therefore shock propagation in the confining medium and the target as well is one-dimensional. The 1-D assumption is appropriate when the size of laser beam, which typically follows a Gaussian distribution, is relatively large. The shock model in this paper made modifications to Fabbro's model assuming the laser beam spot size is in the order of microns. The 1-D assumption is followed but a 2-D equivalence is considered to account for the small laser spot size.

In LSP, a portion of the incident laser intensity *I(t)* is absorbed by the plasma as $I_p(t) = AP(t)I(t)$ where *AP(t)* is the absorption coefficient of the plasma. Assuming a constant fraction α of the absorbed energy be used to increase the thermal energy of the plasma, the following relations between shock pressure *P(t)* and plasma thickness *L(t)* can be derived (Fabbro, et al., 1990):

$$\frac{dL(t)}{dt} = \frac{2P(t)}{Z} \qquad (1)$$

$$(\frac{Z}{2} + \frac{3}{4\alpha})(\frac{dL(t)}{dt})^2 + \frac{3Z}{4\alpha}L(t)\frac{d^2L(t)}{dt^2} = I_p(t) \qquad (2)$$

where $Z = 2/(1/Z_1 + 1/Z_2)$ is the impedance expressed in terms of those of the confining medium (Z_1) and the target material (Z_2). The impedance is the product of density ρ and shock propagation velocity *D*. For instance, the impedance of aluminum, copper and water are 1.5×10^7 kg/m^{2}s, 4.18×10^7 kg/m^{2}s, and 1.65×10^6 kg/m^{2}s, respectively.

If *I(t)*, *AP(t)* and α are constants, shock pressure is found to be proportional to the square root of laser intensity. If *I(t)*, *AP(t)* and α are variables, the peak shock pressure is still proportional to the square root of the peak laser intensity and α. Thus it is reasonable to assume that shock pressure follows a Gaussian spatial distribution with its $1/e^2$ radius proportional to the$1/e^2$ radius of the laser beam. In this way, spatial non-uniformity of shock pressure is considered, which is needed when the laser spot size is small as in this case. The spatially uniform shock pressure *P(t)* relates to the spatially non-uniform shock pressure as

$$P(r,t) = P(t)\exp(-\frac{r^2}{2r_0^2}) \qquad (3)$$

where *r* is the radial distance from the center of the laser beam, and r_0 the radius of laser beam. *P(r,t)* can be solved numerically from the above equations given initial values of *P(t)* and *L(t)*. The values of *P(r,t)* are then used as dynamic shock load in the subsequent stress analysis. A typical dependence relationship of the shock pressure magnitude and duration on laser intensity is shown in Fig. 2.

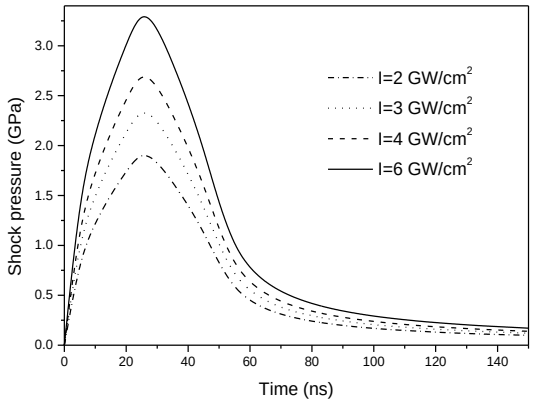

Figure 2 Effects of laser intensity on shock pressure (pulse duration = 50ns and α = 0.2) for water-confined aluminum.

3.2 Stress analysis

The governing equations for stress analysis follow standard elasticity/plasticity analysis except the extremely high pressure and strain rate involved calls for special considerations. The influence of the high strain rate on the yield strength of material has been considered (Meyer, 1992; Johnson, et al., 1983). The influence of pressure on the yield strength of material was found to be more important than other effects when the pressure is larger than 10 GPa and a constitutive model applicable to such high pressures was given by Steinberg, et al. (1980). Steinberg's model did not consider rate dependent effects, however. For shock pressures below 10 GPa, the rate dependent effects cannot be neglected (Zhang and Yao, 2000). In laser shock processing, the pressure involved is fairly high (>1 GPa) but less than 10 GPa. Therefore, both strain rate ef-

fects and shock pressure effects on the yield stress of materials need to be considered. Based on the above mentioned models and assuming that the material compression is negligible in the range of working pressure (below 10 GPa), the following constitutive equations are suggested and used in this paper.

$$G = G_0[1 + (\frac{G_p^{'}}{G_0})P + (\frac{G_T^{'}}{G_0})(T - 300)] \qquad (4a)$$

$$Y = Y_0[1 + C\ln\dot{\varepsilon}][1 + B\varepsilon]^n[1 + (\frac{Y_p^{'}}{Y_0})P + (\frac{G_T^{'}}{G_0})(T - 300)] \qquad (4b)$$

$$G_p^{'} = \frac{dG}{dP}, G_T^{'} = \frac{dG}{dT}, Y_P^{'} = \frac{dY}{dP}, \frac{Y_p^{'}}{Y_0} \approx \frac{G_p^{'}}{G_0} \qquad (4c)$$

where G is the shear modulus, P is pressure, T is temperature, Y is yield strength, Y_0 and G_0 are values at reference state (T = 300 K, P = 1 atm, strain free), C is the logarithmic rate sensitivity at strain rate 1 s^{-1}, ε is strain, $\dot{\varepsilon}$ is strain rate, B and n are the material parameters describing work hardening effect. The primes in Eq. 4 denote derivative with respect to the quantity indicated in the subscribt. As seen from Fig. 3, the influence of high strain rate and high pressure on the yield strength of copper and aluminum is significant (Zhang and Yao, 2000).

4. CONSIDERATIONS IN INTRODUCING THE LSP EFFECT TO LASER MACHINING / MICROMACHINING PROCESSES

If a laser machining/micromachining process is carried out in a confining medium (e.g., water), it may realize the effect of LSP, that is, imparting compressive residual stress into the target material as explained in Section 2. In fact, laser machining underwater or in other liquids were investigated (Watu, et al., 1993; Alfille, 1996). Advantages such as reduced heat-affected zone, reduced debris re-deposition, and beam self-focusing were reported. But the effect of LSP was not observed. This is because the laser intensity used in these studies was not high enough to induce the shock waves as in LSP. If a suitably higher intensity is employed, it is possible to introduce the LSP effect into a laser machining/micromaching process confined in water.

On the other hand, overly high laser intensity may cause water breakdown. When water breakdown takes place, laser energy cannot reach the target surface efficiently and water will lose its function of confinement. The exact level of laser intensity causing water breakdown depends on laser wavelength and the laser-water interaction time. When the laser pulse duration is in the order of nanoseconds, water can stand fairly high level of laser intensity without breakdown, for instance, in the order of 4 GW/cm^2 for laser wavelength of 355 nm (Berthe, et al., 1999).

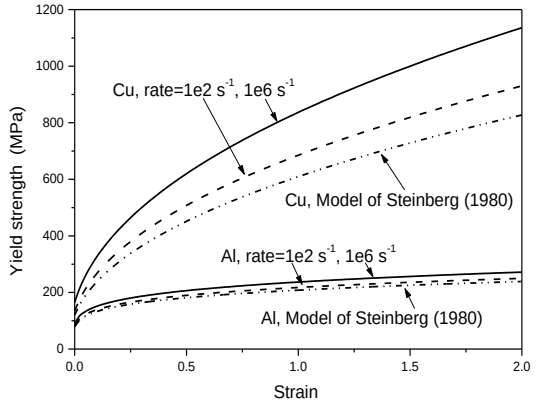

(a)

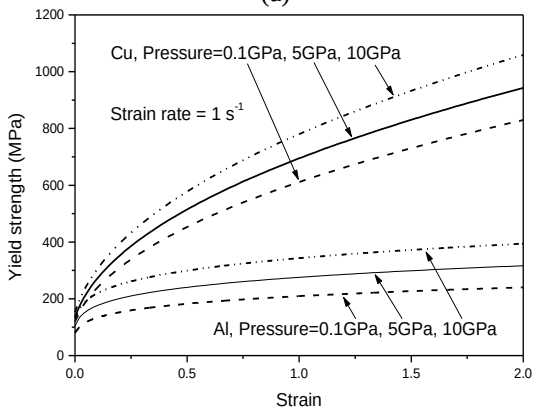

(b)

Figure 3 (a) Influence of strain rate on the yield strength of copper and aluminum (pressure = 1 atm and T = 300 K); and (b) Influence of ultrahigh pressure on the yield strength of copper and aluminum (strain rate = 1 s^{-1} and T = 300 K)

For LSP alone, the number of pulses required usually ranges from one to a very few and the pulse duration used is normally short. If a laser machining/micromachining process employs a pulsed laser source with pulse width in the nanosecond scale and a slow repetition rate, it is perceivably possible to raise the laser intensity to machine and shock process at the same time. The slow repetition rate is required to prevent possible severe water breakdown. But in practice, laser machining/micromachining is usually carried out in either pulse mode with a high repetition rate or in continuous wave mode in order to obtain a reasonable material removal rate.

Another possibility is to carry out laser machining and shock processing sequentially, that is, to apply LSP to a pre-machined part. The part could be machined using laser or other means and has an undesirable residual stress distribution around the machined region. LSP is then used to impart additional stress to result in a more desirable residual stress distribution.

Whether to machine and shock process simultaneously (using a pulsed laser with pulse width in the nanosecond scale) or sequentially, a coating may or may not be applied. With a coating, the shock effect could be enhanced as dis-

cussed earlier. But under the simultaneous machining/shock processing scheme, the benefit of the coating will be realized only during the first few pulses. Once the coating is vaporized, only the confining water helps enhance the shock waves. On the other hand, coating is inconvenient in machining especially in industrial settings and therefore a good compromise perhaps is to use no coating in the simultaneous machine/shock process. Under the sequential machining/shock processing scheme, a coating could be used in the shock-processing phase. But the benefit of enhancing shock waves may be offset by the fact that it is inconvenient to coat the pre-machined features and it becomes more difficult to clean the residual coating around these features after shock processing.

5. EXPERIMENT AND SIMULATION

LSP experiments were first carried out to validate LSP simulation results. Experiments were then extended to laser drilling and grooving confined by water with and without coating. Copper foil of 90-micron thickness and aluminum foil of 70-micron thickness were used as target materials. The foils were made into 10 by 10 mm samples, each of which was adhesively attached to a stainless steel back for rigid support and easy handling. To apply the coating, a thin layer of high vacuum grease (about 10 microns) was spread evenly on the polished sample surface, and the coating material, aluminum foil 16 microns thick, which was chosen for its relatively low threshold of vaporization, was tightly pressed onto the grease. The sample was placed in a shallow container with distilled water around 3mm above the sample (Fig. 1). A frequency tripled Nd:YAG laser in TEM_{00} mode was used (wavelength 355 μm), laser pulse duration was 50 ns, laser repetition rate is 1KHz, and laser beam size is 12 microns. Pulse energy was varied from 160 μJ to 240 μJ corresponding to laser intensity of 2.83 to 4.24 GW/cm^2. After shock processing, the coating layer and the vacuum grease were removed. The geometry of the shocked area was observed using optical microscope, SEM and profilormeter.

LSP simulations were carried out. In the stress analysis, work hardening, strain rate and pressure effects on yield strength (Eq. 4) were considered at room temperature. This is reasonable because only the coating is vaporized and minimal thermal effects are felt by the sample. Shock pressure was computed and used as loading for the 2D axisymmetric stress analysis. A commercial FEM code, ABAQUS, was used to compute the deformation and stress distribution of the sample under the shock pressure. The computation domain is 70 (90) microns in *z*-direction and 1000 microns in *r*-direction for the aluminum (copper) sample (Fig. 1). The radial (11) and depth (22) directions used in Figs. 7 and 9 are defined in Fig. 1. The mesh is denser near the center and the top. The simulation is a dynamic implicit nonlinear process. Single and multiple pulses at various energy levels were simulated. The boundary conditions for the axisymmetric stress model are as follows. At the centerline, $d_r = 0$ due to symmetry where d_r is the *r*-axis displacement; at the outer edge, traction free, that is $\sigma_{ij}n_j = 0$, $i, j = r, z$; at the bottom surface, fixed in position, that is, $d_z = 0$, $d_r = 0$ and d_z is the *z*-axis displacement; and at the top surface, surface traction equals the applied shock pressure, that is, $\sigma_{ij}n_j = P(r,t)$, $i, j = r, z$.

LSP of samples with a pre-drilled hole on the top surface was also simulated to examine the effects of shock pressure on the stress distribution around the hole. Thermal effects were again neglected under this sequential machining/shock processing scheme. The computation domain is the same as the above except that a blind hole (radius = 10 μm, depth = 20 μm) was assumed at the top surface coaxial with the symmetrical axis. At the bottom of the hole and the top surface of the sample, surface traction equals the applied shock pressure, that is, $\sigma_{ij}n_j = P(r,t)$, $i, j = r, z$. At the wall of the hole, $\sigma_{ij}n_i = P(r=10\ \mu m, t)$, $i, j = r, z$, because of the blindness of the hole. The other boundary conditions are the same as above.

6. RESULTS AND DISCUSSIONS

6.1 Experimental validations of LSP modeling

Fig. 4 shows a typical SEM micrograph of dents made on aluminum surface using LSP. Each dent was produced by 3 laser pulses with pulse energy E=240 μJ (I=4.24 GW/cm^2). The holes shown on both sides of the figure were drilled for locating purpose. Fig. 5 shows the SEM micrograph of dents made on copper surface using LSP under the same condition. Note the difference in magnification and the dents on aluminum in fact are much larger and deeper than that on copper due to the lower yield strength of aluminum (Fig. 3). As seen, the dents are quite visible under the SEM and are evidence of plastic deformation.

The geometry of the dents was measured using a profilometer and compared with simulation results. Comparison between experiments and simulations in terms of dent depth is shown in Fig. 6. As mentioned, aluminum has larger deformations than copper given the same process condition because aluminum's yield strength is lower. As the pulse number increases from 2 to 6 the dent depth increases almost linearly (Fig. 6 (a)). This is due to the fact that subsequent pulses see almost the same geometry on the target as previous ones since the deformation is small. On the other hand, when pulse energy increases the increase of the dent depth is faster (Fig. 6 (b)). This is because when the pulse energy increases, both the level of shock pressure and the duration of the pressure increase as seen in Fig. 2. The relatively large deviations at 5 to 6 pulses were due to thermal effects because the coating layer was too thin to totally isolate the thermal effects when the number of pulses increases.

In general, experimental results agree well with simulation predictions for both aluminum and copper under various conditions.

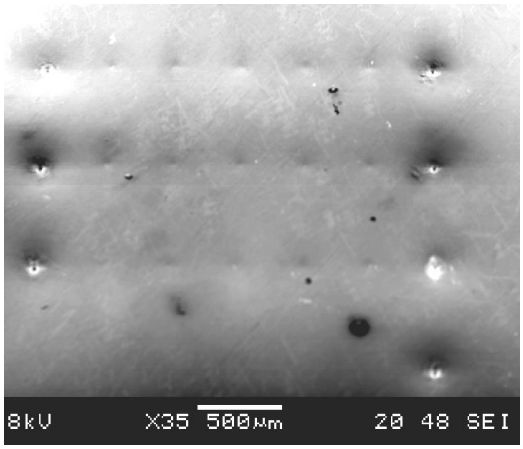

Figure 4 SEM micrograph of dents produced by LSP on aluminum sample (3 laser pulses at each location with pulse energy E = 240 μJ, laser pulse duration = 50 ns, pulse repetition rate = 1 KHz, beam diameter = 12 microns, laser wavelength = 355 nm)

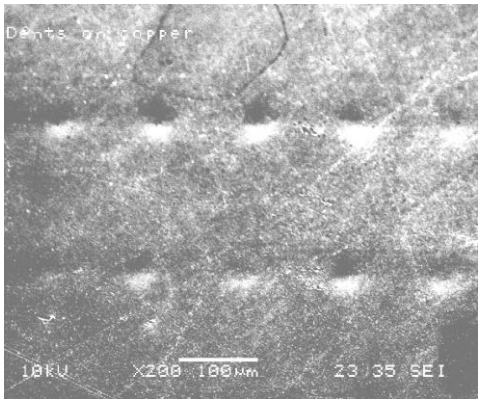

Figure 5 SEM micrograph of dents produced by LSP on copper sample (under the same condition as stated in Fig. 4)

6.2 Residual stress

Fig. 7 shows a typical distribution of residual stresses for a single pulse with pulse energy E = 200 μJ (I = 3.54 GW/cm^2). The computation domain is 70 microns by 1000 microns, and the region shown is 70 microns by 150 microns for viewing clarity of the area heavily stressed. As seen from Fig. 7 (a), radial stress *S11* is compressive in a wide region below the top surface with the maximum of 148 MPa reached along the centerline and about 60 microns into the sample. On the top surface, *S11* is compressive within 10 microns from the center and is tensile in the range of 10 to 35 microns, and then becomes compressive again. Such tensile radial stress near the edge of laser irradiation was also observed in LSP using large beam sizes (Clauer, et al., 1981). This thin layer of tensile stress is undesirable, but can be altered by overlapping laser pulses at proper spacing as shown in Fig. 8 (c) where a line of dents were induced by overlapping laser pulses at a uniform spacing of 25.4 microns. The wide range of compressive radial stress near the top surface is desired for the prevention of crack formation and propagation.

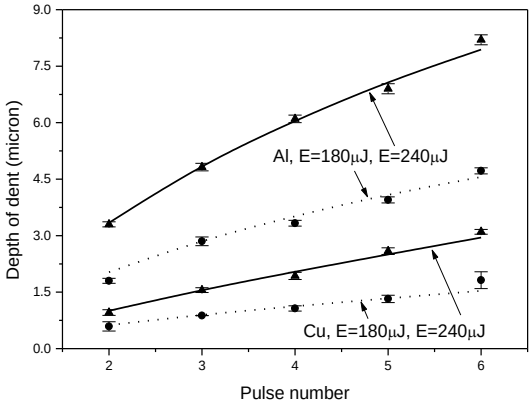

(a)

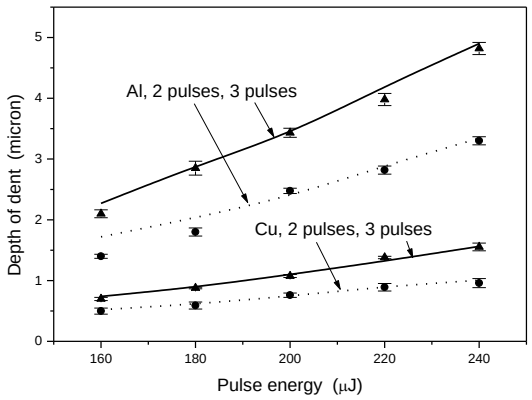

(b)

Figure 6 Geometry comparison between experiments and simulations for copper (thickness = 90 microns) and aluminum (thickness =70 microns) (a) Dent depth vs. pulse number, E = 180 μJ and 240 μJ; and (b) Dent depth vs. pulse energy, pulse number = 2 and 3. The error bars represent standard error.

Fig. 7 (b) shows the distribution of in-depth residual stress *S22*. *S22* is close to zero near the top surface as expected from the equilibrium requirement, and becomes compressive at the lower center part of the sample. The locations of the maximum tensile and compressive in-depth residual stresses are close to the bottom surface instead of the top surface. One explanation is that the bottom surface is fixed in position, while the top surface is traction free when the shock load is removed. The top part of the sample will have nearly zero in-depth stress after sufficient stress relaxation, but the center bottom part cannot relax as the top surface does because both the centerline and the bottom surface are fixed in position. As a result, the in-depth residual stress accumulates near the center bottom region.

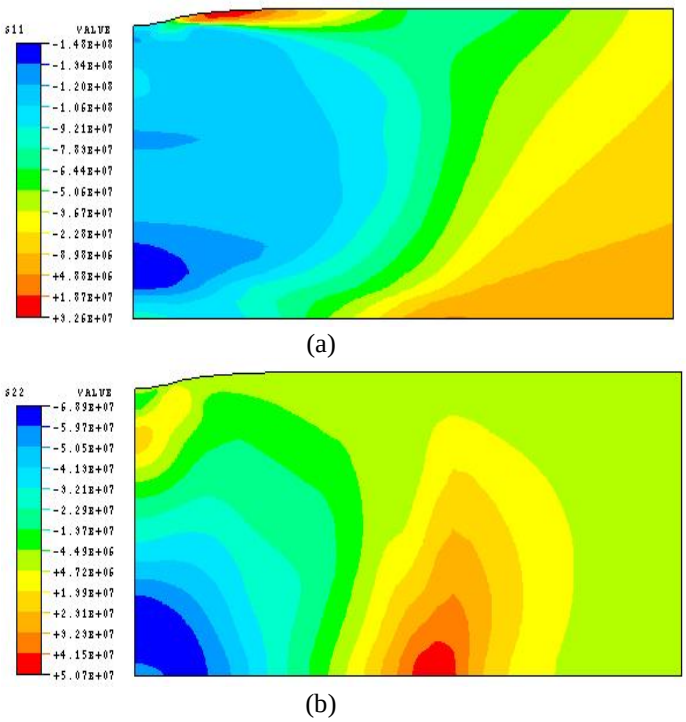

(a)

(b)

Figure 7 (a) Radial residual stress *S11;* and (b) In-depth residual stress *S22*. Aluminum, E=200 μJ (I=3.54 GW/cm^2), AP=0.545, and α=0.2. Computation domain is 70 microns by 1000 microns, and the region shown is 70 microns by 150 microns for viewing clarity. The deformation is magnified by a factor of 3 for viewing clarity. Stress unit: Pascal. The axial directions are as defined in Fig. 1.

6.3 Feasibility study results of introducing LSP effects into laser micromachining

Laser drilling and grooving experiments confined by water were carried out to explore the feasibility of introducing the LSP effect into laser micro-machining. Laser beam size was 12 microns and Laser intensity was chosen as 4 GW/cm^2. Fig. 8(a) and (b) show through-holes drilled with and without coating on the aluminum sample of 70-micron thickness. 45 laser pulses were used. The area surrounding the hole was obviously dented and clearly indicates surface compression took place as in LSP. Such dented regions were not observed in open-air or previously reported underwater laser machining research work. The hole drilled with coating (Fig. 8(a)) shows stronger denting than the hole drilled without coating (Fig. 8 (b)) because of coating-enhanced shock effect, although the hole drilled with coating has a rougher surface perhaps left there by burnt grease or coating.

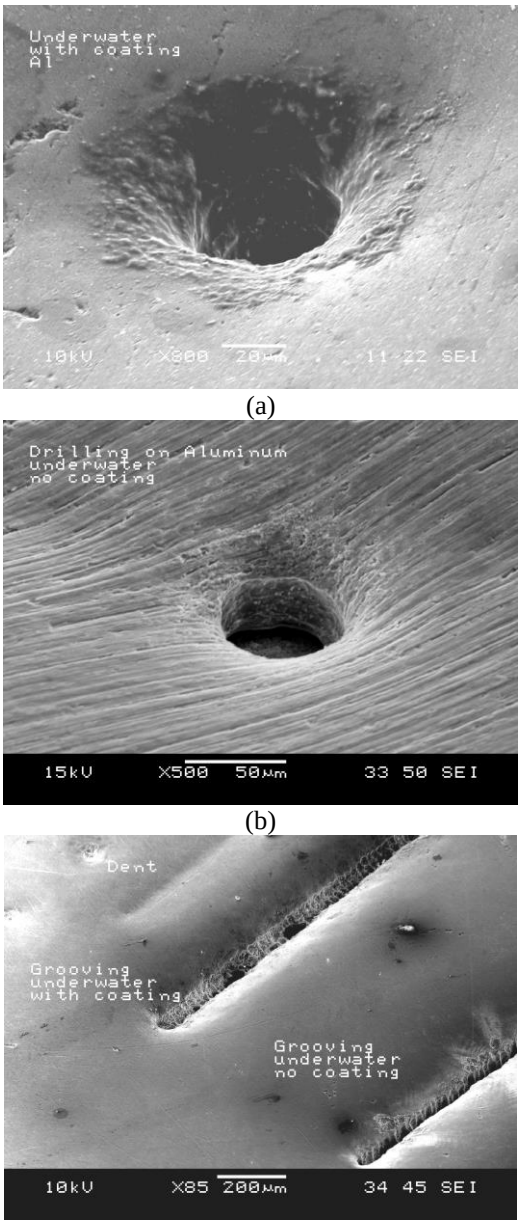

(a)

(b)

(c)

Figure 8 (a) Laser drilling confined by water with coating; (b) Laser drilling confined by water without coating; and (c) Laser grooving confined by water with and without coating. Aluminum sample thickness = 70 μm. Pulse energy E = 230 μJ (I = 4 GW/cm^2), pulse duration = 50 ns, beam diameter = 12 μm. Holes were drilled with 45 pulses. Grooves were formed by a series of holes uniformly spaced at 25.4 μm and each hole was drilled with 24 pulses. Laser pulse repetition rate = 1KHz.

Fig. 8(c) shows the results of laser grooving on aluminum sample of the same thickness. 24 pulses were applied at a location before the laser beam moved to the next adjacent location 25.4 microns apart. The process was repeated until a groove was formed. The reason of using this scheme instead of continuously moving the beam is to prevent con-

tinuous interaction of laser and water and possible water breakdown. Note the areas around the grooves were visibly dented and again indicate strong compression took place. Grooving with coating produced slightly deeper dented area around the groove than grooving without coating. Compared with open air drilling and grooving, laser drilling and grooving confined by water at a proper laser intensity level produced cleaner top surfaces and visibly dented area around the machined region. This is indicative of the potential of achieving high quality machining results along with substantial compressive residual stress distributions by introducing the LSP effect into laser machining / micromachining.

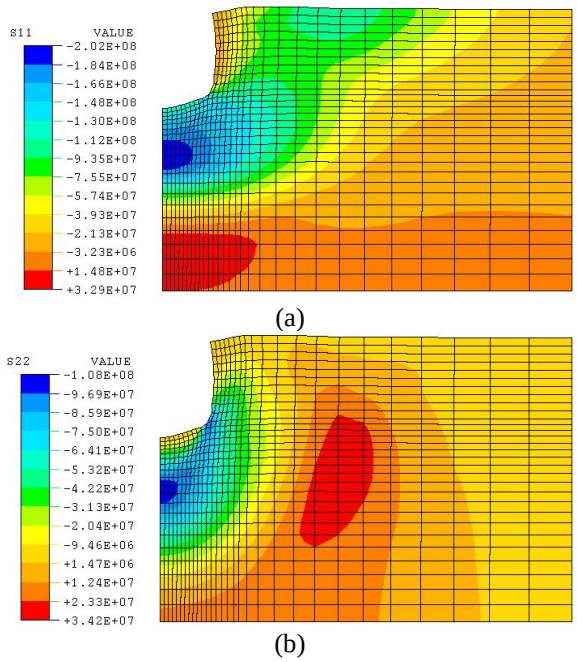

Figure 9 Typical distribution of residual stresses on aluminum sample with a predrilled blind hole (radius = 10 μm, depth =20 μm) (a) radial residual stress *S11*; and (b) in-depth residual stress *S22*, E = 230 μJ (I = 4 GW/cm^2), beam diameter = 12 μm. Stress unit: Pascal. Axisymmetry is assumed. The region shown is 70 by 100 μm. Deformation is magnified by a factor of 3 for viewing clarity. (The axial directions are as defined in Fig. 1)

Simulation was carried out for LSP of samples with a pre-drilled blind hole to mimic the sequential machining/shock processing scheme. The boundary conditions and the location and size of the hole was described in Section 5. Pulse energy E is 230 μJ, corresponding to the 4 GW/cm^2 laser intensity used in experiments of underwater laser drilling and grooving. Although thermal effects and initial stresses were not considered, these simulation results provide preliminary feasibility assessment of the scheme. As seen, under the action of shock pressure, plas tic deformation was induced around the surface of the hole

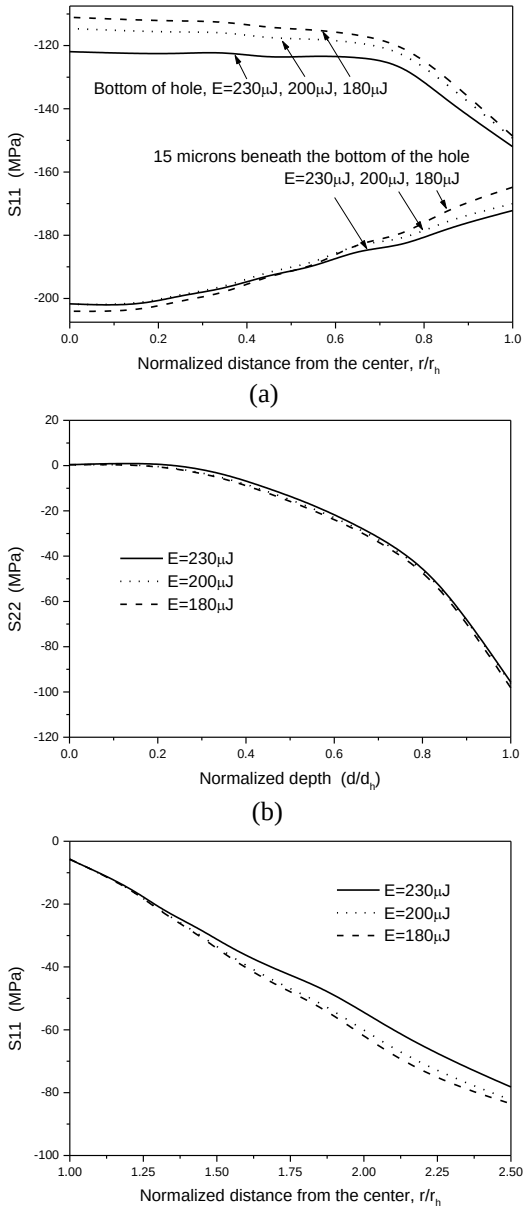

Figure 10 Influence of energy level on the distribution of (a) radius residual stress *S11* on the bottom surface of the hole and at 15 microns below the bottom surface of the hole; and (b) in-plane residual stress *S22* along the wall of the hole, and (c) radial residual stress *S11* on the top surface. Distance from the center is normalized to the radius of the hole r_h and r_h = 10 μm. Location of points on the wall from the top surface is normalized to the depth of the hole d_h and d_h = 20 μm (Fig. 9).

(Fig. 9). Radial residual stress *S11* is compressive around the hole. The compressive region extends 30 microns downward from the bottom of the hole and 100 microns outward from the centerline (Fig. 9(a)). Maximum compressive radial residual stress (about –202 MPa) is reached around 15 microns below the bottom of the hole. In-depth residual stress is close to zero on the top surface as ex-

pected from the equilibrium requirement, but beneath the bottom of the hole it is compressive (Fig. 9 (b)). Such residual stress distribution is desired for the purpose of crack prevention.

As shown in Fig. 10 (a), the compressive radial residual stress *S11* on the bottom surface of the hole increases with the increase of pulse energy. These values were extracted from Fig. 9. The compressive radial stress also increases as it goes close to the bottom corner of the hole (i.e., $r/r_h \rightarrow 1$), where r_h is the radius of the hole (10 microns). At 15 microns below the bottom surface of the hole *S11* is more negative than on the top, and the stress at this depth does not change with energy as much as the bottom surface of the hole does. These are due to the work hardening effects and the 3D propagation of the shock waves inside the material. Fig. 10 (b) shows the distribution of *S22*, which is the in-plane stress along the vertical wall of the hole. It is seen that *S22* is close to zero at the top corner due to equilibrium requirement and becomes more negative as it moves downwards. The bottom corner of the hole shows strong stress accumulation, but both *S11* from the bottom surface and *S22* from the wall are compressive around this corner. Shown in Fig. 10 (c) is the radial stress around the top surface, which is all compressive. In summary, the simulation shows that extensive compressive residual stresses can be induced around the hole. The in-plane residual stress for both the bottom and top surfaces of the hole, as well as in-plane stress along the wall of the hole are compressive or very close to zero. Such stress distribution is desired for prevention of micro crack propagation.

7. CONCLUSIONS

Based on a brief review of principles and model of laser shock processing, the possibility of introducing the LSP effect, that is, imparting compressive residual stress distribution into the target material, to laser micromachining processes were discussed and its feasibility were experimentally and numerically investigated. The LSP model was properly modified to suit for the micro scale, and the effects of high strain rate and ultrahigh pressure were considered in the stress analysis. It is shown that both simultaneous and sequential micromachining/shock processing are feasible. Under both schemes, significant compression was observed. Under the simultaneous scheme, it is important to keep the repetition rate of a pulsed laser source low to avoid possible water breakdown but this may impair the material removal rate of the process.

8. ACKNOWLEDGEMENTS

Support for this project from NSF under grant DMI-9813453 and equipment support from ESI are gratefully acknowledged.

9. REFERENCES

Alfille, et al., 1996, "New pulsed YAG laser performance in cutting thick metallic materials for nuclear applications," *SPIE*, 1996, Vol. 2789, pp. 134-144.

Berthe, L., et al., 1999, "Wavelength dependent of laser shock-wave generation in the water-confinement regime," *J. Appl. Phys.*, June, 1999, Vol. 85, pp. 7552-7555.

Clauer, A. H., et al., 1981, "Effects of laser induced shock waves on metals," Shock Waves and High Strain Phenomena in Metals-Concepts and Applications, New York, Plenum, 1981, pp. 675-702

Fabbro, R., et al., 1990, "Physical study of laser-produced plasma in confined geometry," *J. Appl. Phys.*, July, 1990, Vol. 68(2), pp. 775-784.

Fox, J. A., 1974," Effect of water and paint coatings on laser-irradiated targets," *Appl. Phys. Lett.*, 15 May 1974, Vol.24, No. 10, pp. 461-464.

Johnson, G. R., et al., "Response of various metals to large torsional strain over a large range of strain rates," *J. Eng. Mat. Techn.*, Jan. 1983, Vol. 105, pp. 42-53.

Li, K. and Sheng, P. S., 1995, "Computational model for laser cutting of steel plates," *Manufacturing Science and Engineering*, ASME 1995, MED-Vol. 2(1), pp.3-14.

Meyer, L. W., 1992, "Constitutive equations at high strain rates," Shock-wave and High-Strain-Rate Phenomena in Metals, Marcel Dekker, Inc., New York, 1992, pp. 49-68.

Modest, M. F., 1997, "Thermal elastic and viscoelastic thermal stresses during laser drilling of ceramics," *J. Heat Transfer*, 1997, Vol. 120, pp. 892-898.

Modest M. F., and Mallison, T. M., 1999, "Transient elastic thermal stresse development during laser scribing of ceramics," *ICALEO 1999*, pp. B118-127.

Peyre, P., et al., 1996, "Laser shock processing of materials, physical processes involved and examples of applications," *Journal of Laser Applications*, 1996, Vol. 8, pp.135-141.

Sheng, P. S. and Joshi, V. S., 1995, "Analysis of heat-affected zone formation for laser cutting of stainless steel," *Journal of materials Processing Technology*, 1995, Vol. 53, pp. 879-892.

Steinberg, D. J., et al., 1980, "A constitutive model for metals applicable at high-strain rate," *J. Appl. Phys.*, March 1980, Vol. 51(3), pp. 1498-1504.

Watu, D, et al., 1993, "Laser hole drilling under nonlinear liquid mediums," *ICALEO(1993)*, pp. 59-69.

Zhang, W. and Yao, Y. L., 2000, "Improvement of laser induced residual stress distributions via shock waves," *ICALEO'2000, Laser Material Processing*, Vol. 89, pp. E183-192.